

Contents lists available at ScienceDirect

Applied Energy

journal homepage: www.elsevier.com/locate/apenergy





Design and experiments of a thermoelectric-powered wireless sensor network platform for smart building envelope

Qiliang Lin^a, Yi-Chung Chen^b, Fangliang Chen^c, Tejav DeGanyar^c, Huiming Yin^{a,*}

- ^a Department of Civil Engineering and Engineering Mechanics, Columbia University, United States
- Department of Electrical and Computer Engineering, Tennessee State University, United States
- ^c Virtual Construction Lab of Schüco, United States

HIGHLIGHTS

- First self-powered wireless sensing platform entirely inside the window frame.
- Milli-watt level power management with thermoelectric energy harvesting.
- Energy equilibrium analysis proposed for the self-powered design at any location.
- Platform robust to various sensors and contributes the smart building envelope.

ARTICLE INFO

Keywords: Smart building envelope Energy harvesting Wireless sensor platform Energy equilibrium design

ABSTRACT

A new thermoelectric-powered wireless sensor network platform is presented for the low-cost environmental sensing in building envelopes through thermoelectric energy harvesting and ultra-low power management. It is designed and prototyped entirely inside a window frame without compromising architectural aesthetics. This self-powered sensing platform is achieved by maximizing the harvested energy from building envelopes and optimizing the wireless sensing unit's energy consumption. It harvests milli-watt level thermoelectric power from the temperature gradient across building envelopes through thermoelectric generators with an optimized thermal connector. The harvested energy is voltage-boosted and regulated through two integrated circuits that are tailored for ultra-low-power input. A low power system-on-chip is used to supervise the environmental sensing and wireless data communication. The energy consumption is tailored by adjusting the system sleep time to match the harvested energy. The proposed platform is prototyped in a window frame and thoroughly tested, where 1.5 mW of power is harvested from thermoelectric generators under 6 °C of temperature difference, and a 33.4% efficiency to the battery. In the meantime, 0.42 mW power is consumed by the wireless sensing unit under a sampling period of 2 h, which reaches the energy equilibrium state. The energy equilibrium algorithm can project the battery energy based on historical weather conditions, so as to achieve the self-powered condition given a geographic location. This smart building envelope systems include the unique innovations in selfpowered system architecture, thermally optimized internal structure, and milli-watt level power management.

1. Introduction

A grand challenge emerging in the energy system is to address the critical national needs of energy security, economic competitiveness, environmental responsibility, smart serviceability, and workability simultaneously. The building sector is the largest consumer of electricity. It was reported that the buildings sector accounts for about 76% of electricity use and 40% of all United States primary energy use and

associated greenhouse gas (GHG) emissions [1]. Globally, about 30% of total energy and 60% of electricity are consumed on buildings [2]. The primary energy consumptions in buildings are heating, ventilation, air conditioning, lighting, and other major appliances (water heating, refrigerators, dryers, etc.) [3]. The share of electricity use in building sectors has grown dramatically from 25% of the United States annual electricity consumption in the 1950 s to 40% in the early 1970 s, and to more than 76% by 2012 [1]. In this sense, smart building management

E-mail address: yin@civil.columbia.edu (H. Yin).

 $^{^{\}ast}$ Corresponding author.

becomes significantly important to achieve optimal interior comfort with minimal energy expenditure. The smart building concept emerged at the beginning of the 1980 s and has been continuously evolving during the past decades [4–6], where the ability to adapt to the dynamic environments is considered as the central aspect in its definition [7]. Research shows that a potential energy saving of 34.78% could be achieved by the smart buildings comparing to conventional buildings, through the optimal control of major building components like the heating, ventilation, air conditioning, and lighting systems [8].

The concept of the smart building has attracted significant attention in the civil engineering industry during the past decade and is estimated to worth 53.45 billion by 2022 [9]. Significant attention has been paid to the controlling algorithms of the smart building management systems (BMSs) thanks to the boom of artificial intelligence, with many discussions about energy consumption forecast [10-12], smart grid technology [13], and in-room occupancy detection [14]. In contrast, the importance of the sensor network was underestimated with fewer research and discussions. Traditional systems rely heavily on wired sensors to monitor the environment, which comes with substantial workforce and time in both installation and maintenance. Therefore, the concept of the wireless sensor network (WSN) becomes more and more popular in BMSs to ease the installation and maintenance, to enhance the flexibility in dangerous areas, and to reduce the cost of sensor deployments [15]. However, most of these sensors are powered by either replaceable or rechargeable batteries, which means they are exposed to limited battery life, environmental hazards, and complex replacement procedures [16]. For certain applications in the building environment, it could be difficult to replace the battery of WSN and could result in an enormous scale of maintenances cost.

The energy harvesting technologies provide an excellent solution to elongate the battery life and reduce the maintenance cost of a WSN such that the self-powered wireless sensor network (SPWSN) system can be achieved. Energy harvesting technologies use power generating elements such as solar cells [17], piezoelectric elements [18], electromagnetic components [19,20], and thermoelectric elements [21] to convert light, pressure, vibration, and heat energy into electricity. A comprehensive review of energy harvesting applications in the buildings can be found in [22], from which photovoltaics and thermoelectricity are two primary energy sources for the WSN systems in buildings. A solar energy based SPWSN was proposed by Tzortzakis et al. [23] for the environmental monitoring and smart city design, with the corresponding field test conducted on the campus of the National Technical University of Athens. The solar panels provided abundant energy supply up to 3.5 W but also resulted in a relatively bulky size of the prototype. Moreover, since solar energy enjoys a much higher power output than other energy harvesting sources, the proposed system is not robust to the cases where solar energy is not available. The thermoelectric (TE) energy serves as a potential alternative when solar energy is not available. Compared to solar energy, TE energy harvester suffers from much lower power and voltage output, which cast challenges to the conversion efficiency and energy equilibrium for the WSN. Recently, a new TE energy harvester for the building energy management WSN was proposed by Wang et al. [24] by harvesting the wall-mount heater with 60 °C surface temperature, and a 25% end-to-end efficiency was achieved with 1.7% duty cycle. A higher efficiency TE-based WSN system is later proposed by Guan et al. [25], with the end-to-end efficiency ranging from 44.2% to 75.4% under different open-circuit voltages. The system was built based on a two-stage boosting scheme with tens of microwatts to several milliwatts power input from thermoelectric generators (TEGs). However, both systems mentioned above are tested in the lab and did not discuss the potential applications in the building industry.

The building envelopes, as the skin of buildings and the main barrier against the external environment, are crucial to the environmental sensing and energy harvesting [26]. Some well-known applications include the building integrated photovoltaic-thermal roofing systems [27], sun-powered smart window blinds [28], and wind energy

harvester inside double-skin façades [29]. However, for sensing applications inside building envelopes, no physical energy source, such as solar or wind, is available. This limitation creates challenges to energy harvesting and WSN applications for the building envelopes. The traditional building envelope designs tend to break the heat transfer and minimize the thermal infiltration by stacking as many thermal resistant materials as possible. Therefore, a thermal break up to 25°C can be easily formulated across the profile, as is schematically shown in Fig. 1. The temperature difference across the building envelope could provide tens of micro-watt to a few milli-watt level of thermal energy harvesting and is a good power supply for WSN nodes. However, due to the challenges of thermal energy harvesting, i.e. the ultra-low power and voltage output, and the limited space inside building envelope profile, no study or design of self-powered WSN system has been observed in the building envelopes.

In this paper, a thermoelectric-powered wireless sensor network (TPWSN) platform is proposed for low-cost environmental sensing in building envelope components and is prototyped into a building window system. The platform is designed entirely inside the window frame with no wired connections to the outside and therefore has no visual compromise to the window's architectural aesthetics. To the best of the authors' knowledge, it is the first self-powered WSN system inside the building window systems and robust to other building envelope structures such as façades and roofs. With a slight modification of the window structure and a minor compromise of its thermal performance, the platform takes advantage of the temperature difference across the window frame for the thermoelectric energy harvesting. It achieves the energy equilibrium between the consumption and the harvesting, which significantly elongates the limited battery life of traditional WSN systems. In energy harvesting, a thermally optimized energy harvesting structure is proposed inside the limited space of window frame for an optimal power output, which is supported by heat transfer analysis through the finite element method. The milli-watt level thermoelectric power is voltage-boosted and regulated through two integrated circuits tailored for ultra-low-power input. In the meantime, a low power system-on-chip (SOC) is applied to supervise the environmental sensing and wireless data communication, and is thoroughly tested for efficiency and energy consumption. The total energy consumption is tailored by adjusting the system sleep time to match the harvested energy so that the self-powered design could be realized. Comprehensive discussions of the design methodologies and experimental validations are elaborated for energy harvesting and the wireless sensor subsystems. An energy equilibrium algorithm based on the test performance is proposed to predict the battery energy level and achieve the self-powered design by properly engineering key design parameters. The self-powered system architecture and energy equilibrium algorithm, the thermally optimized

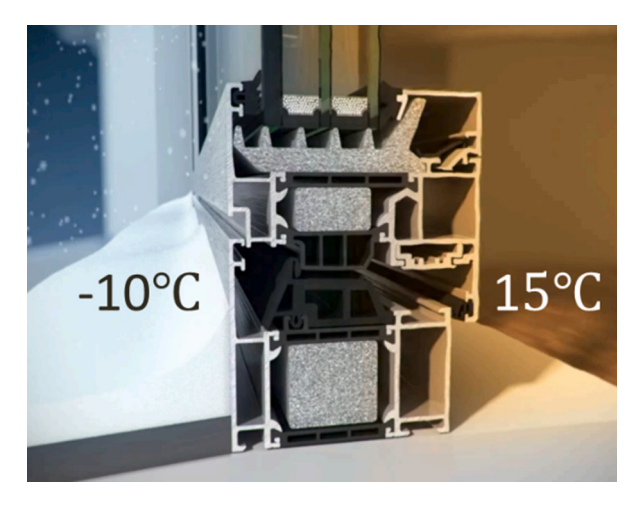


Fig. 1. Thermoelectric energy across the building envelope.

internal structure, and the milli-watt level power management of the proposed TPWSN serve as valuable references and guidance to the design and applications of the next generation smart building envelope systems.

The rest of the paper is organized as follows. Section 2 focuses on the architecture and the design philosophy of the TPWSN system. The energy availability across the window profile and the thermally optimized harvester are first analyzed and designed in Section 2.1. The energy harvesting subsystem and wireless sensor network subsystem are designed and discussed in Section 2.2 and Section 2.3. The energy equilibrium algorithm is theoretically formulated in Section 2.4 based on the key design parameters to aid the self-powered design. In Section 3, the subsystems are integrated into the window frame and tested under a controlled temperature gradation, where the amounts of energy consumption and energy harvesting are continuously monitored and calculated. Section 4 presents the energy equilibrium design and the battery energy prediction based on the case study of the historical temperature data in New York City to theoretically achieve eternal battery life. Such a self-powered design could be extended to any location with proper engineering of the key parameters. Section 5 discusses the cost analysis and potential limitations of the TPWSN system under real applications. Section 6 summarizes the paper with conclusive remarks.

2. System architecture, design, and analysis

The architecture of the SPWSN system is schematically shown in Fig. 2, which consists of an energy harvesting subsystem and a wireless sensor network subsystem. The energy harvesting subsystem contains harvesters for energy conversion, energy management circuits for optimal energy extraction and regulation, and rechargeable batteries for permanent energy storage. The harvested energy is consumed by the wireless sensor network subsystem, which is made of sensors, microprocessors, and wireless communication systems. The microprocessors are connected to both the sensors for environmental monitoring and the wireless communication system for data transmission. The data from a system node will be sent out to an external server for permanent storage, which will serve as valuable information for the optimal heating, ventilation, and air conditioning (HVAC) control and building management. In an ideal SPWSN, the energy harvesting subsystem should

collect as much energy as possible and stabilize the dynamic power source into batteries; whereas the wireless sensor network subsystem should consume as little energy as possible to achieve the energy equilibrium while fulfilling the function in environmental sensing and wireless data transmission.

The thermoelectric powered WSN follows the architecture of a general SPWSN and uses the thermoelectric generator (TEG) as the energy harvester. A TEG is usually made of many thermocouples that could generate electrons under thermal gradients. In the meantime, the building envelope, as the building's skin, is designed to keep the internal environment stable. Therefore, large temperature differences could be easily formulated across the building envelope profiles, thanks to the original thermal-breaking structures like the thermal isolator and the thermal resistive foam. The abundant thermal energy could be harvested via the TEGs to serve the energy consumption of WSN units, so as to formulate a thermoelectric-powered WSN system.

In the scope of this research, the Schüco AWS 75 window system is used for the prototype, which has an internal structure shown in Fig. 3. The proposed TPWSN system fills the rectangular dashed box in Fig. 3 to

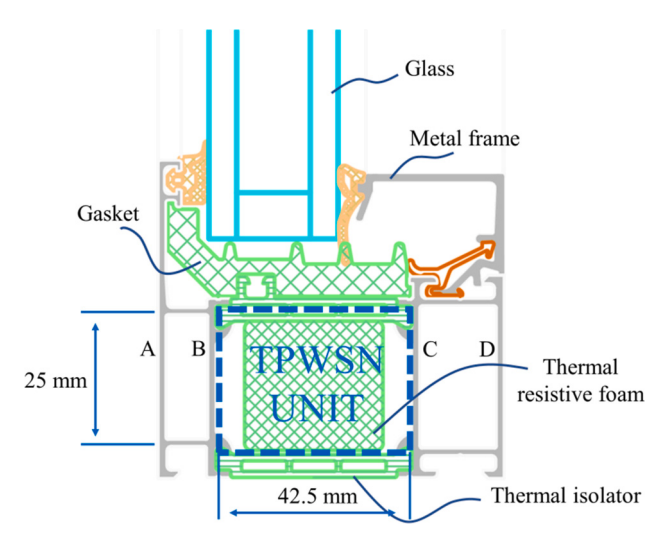


Fig. 3. Schematic design of TPWSN inside a window system.

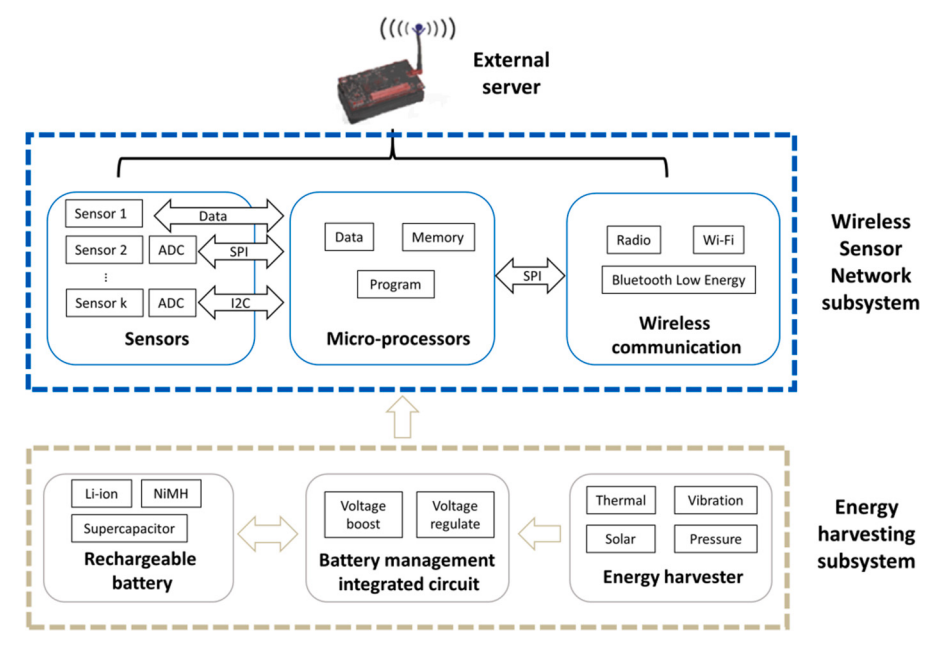


Fig. 2. Architecture of the self-powered wireless sensor network (SPWSN).

replace the original thermal resistive foam. It has physical contact with the B and C surfaces to achieve the maximum thermal conduction and optimal thermal energy harvesting. The detailed design philosophies for both the energy harvesting subsystem and the wireless sensor network subsystem are described in the following subsections.

2.1. Energy harvesting subsystem

2.1.1. Energy harvester

The thermoelectric generators harvest the thermal energy from building envelopes for WSN systems. In order to achieve the optimal energy harvesting, the temperature difference across the window profile must be efficiently directed to TEG surfaces. However, the TEG's thickness is usually limited to 2–4 mm to avoid the buckling of its thermocouples, which means TEG itself is not possible to fill the 42.5 mm cavity in Fig. 3. Therefore, an energy harvester with a thermally optimized internal connector is needed to efficiently transport the thermal gradient from window frames to TEG surfaces. The design philosophy of the energy harvester is discussed in this subsection.

From a single TEG's perspective, its power output depends on the number of thermocouples and individual thermocouple's harvesting power. The harvesting power of a single thermocouple is the product of the voltage and current, both of which are linearly proportional to the applied temperature difference ΔT_{TEG} . The number of a TEG's thermocouples depends on the TEG's size, which is equivalent to its surface area A_{TEG} because the thickness is usually fixed. Therefore, the overall power output is related to the surface area and temperature difference as below:

$$P_{TEG} \propto A_{TEG} \cdot (\Delta T_{TEG})^2 \tag{1}$$

One can simply fill the space with thermally conductive materials, like metals, to transport the maximum temperature gradient from window frames to TEG's surfaces. However, such design introduces significant amount of extra material to the system and impacts other design parameters such as the material cost and window's operating efficiency. Therefore, the weight of the thermal connectors, ω_{TC} , must be considered in the design. A new metric is defined as follows to evaluate the performance of an energy harvester:

$$Eva = \frac{A_{TEG} \cdot (\Delta T_{TEG})^2}{(\omega_{TC})^{\alpha}} \propto \frac{P_{TEG}}{(\omega_{TC})^{\alpha}}$$
 (2)

where α is a scaling factor that indicates the importance of the weight comparing to the power output. The larger the value of α , the more important the weight of the connector. The ideal thermal connector should generate the maximum TEG power output and have the minimum additional weight, and thus maximize the evaluation metric in Eq. (2). It should also fit into the limited space inside the window frame. Therefore, different designs are proposed and analyzed with commercial Finite Element (FE) software ABAQUS to maximize the evaluation metric

Since both the area A_{TEG} and the temperature difference ΔT_{TEG} depend on how the TEG is placed, five difference placement designs shown in Fig. 4 are modeled, with the TEG-vertical angle ranging from 0° to 60° (maximum) at an increment of 15°. In the meantime, four different internal structures are investigated from pure solid, three-bridge, one-bridge, and hollow structures, as illustrated in Fig. 5. The wall thickness and bridge width are prescribed as 1.5 mm. The TEG thickness is prescribed at 3 mm, which is the most common thickness in the market. The 2D profiles are extruded for 60 mm to formulate the 3D FE models for the analysis. Therefore, a total of 20 different models are constructed for heat transfer analysis.

The heat transfer through the thermal connector witch air cavity generally includes convection, conduction, and thermal radiation. Radiation becomes considerable with a large temperature difference, which does not exist here, so it is not considered in the present FE

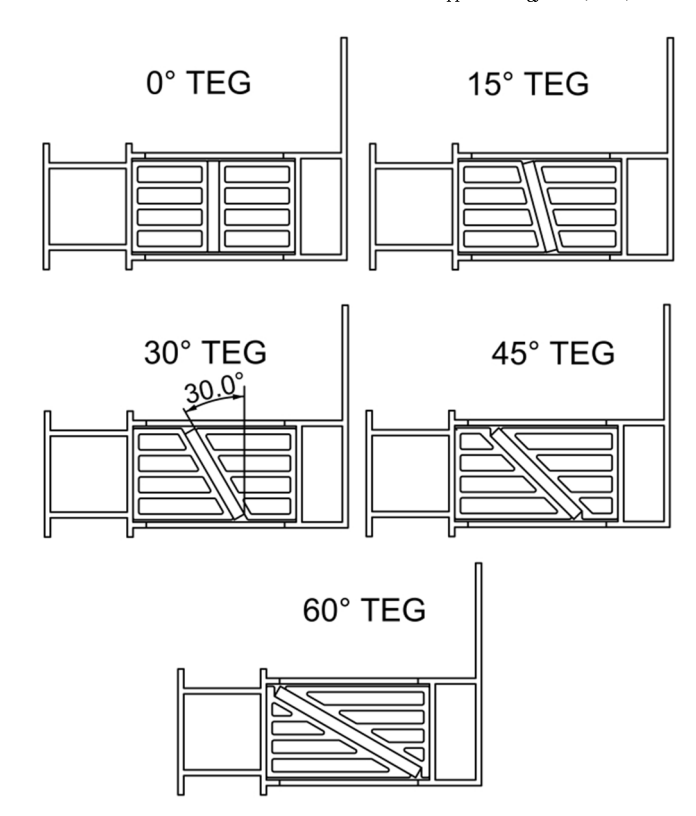


Fig. 4. Three-bridge thermal connector designs with different angles.

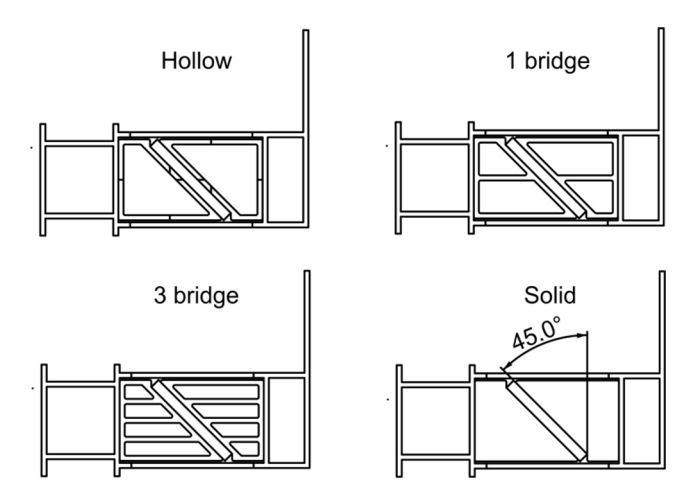


Fig. 5. 45 °C degree thermal connector designs with different internal structure.

analysis. Convection is usually the dominant form of heat transfer in liquids and gases. It involves both heat diffusion (conduction) and advection caused by the motion of the fluid. For air cavities with a smaller than 50 mm distance, the heat transfer from advection is usually smaller than diffusion [30]. In window applications, the air cavities are sealed to avoid leakage and compromise of thermal performance. Therefore, the bulk motion of air inside the cavity is very limited. The thermal conductivities of the metal (aluminum) frame, TEG, thermal isolator (PA66), and air are listed in Table 1. Although the air in the cavities may move internally with a temperature gradient, which leads to a Nusselt number greater than 1 [39], because the thermal conductivity of the air is so low in comparison with the aluminum (0.026 versus 160), the advection effect of air flow is neglected in the FE model. The steady state heat conduction analysis is conducted for the twenty

Table 1Thermal conductivities of materials in the finite element model.

Materials	Aluminum	TEG	Thermal isolator (PA66)	Air
Thermal conductivity (W/m-K)	160	1.7	0.3	0.026

proposed designs, and the FE configuration of the three-bridge 45 °C design is shown in Fig. 6. The in-room side of the aluminum frame is applied with 25 °C fixed temperature boundary, while the out-of-room side is applied with $0^{\circ}C$.

The TEG's surface temperature is extracted from the central plane of all the 3D Finite Element models and plotted for comparison. For simplicity, examples from different thermal connector designs and placement angles are selected, and the temperature profiles on the two surfaces of TEG are plotted in Fig. 7 and Fig. 8, respectively. Fig. 7 shows the temperature profiles under different TEG placement angles for the three-bridge design, while Fig. 8 shows the temperature profiles under different thermal connector designs when the placement angle is 45 °C. The normalized location, which is defined as the point location over the TEG length, is used since different TEG placement angles will have different TEG length. It is seen in Fig. 7 that the temperature difference ΔT_{TEG} reduces with the increase of the placement angle, but the temperature distributions under each angle follow the same trend and are almost in parallel. It is observed in Fig. 8 that the temperature distributes uniformly over the surface for the solid connector design and follows a parabolic trend for the hollow connector design. The outlying points are because of the edge effect and thus are ignored in the analysis.

The temperature difference across the TEG and the thermal connectors' weight are extracted from twenty FE models to calculate the corresponding evaluation metrics under three different scaling factors $\alpha=0,\,0.5,$ and 1. The evaluation metrics are grouped by the scaling factor and normalized, after which they are plotted in Fig. 9 with respect to different placement angles and internal structures. Surprisingly, the best performing angle is always 0 °C under different scaling factors. It is because that the tilted TEG also reduces the temperature difference, although they slightly enlarge the contact surface. The contact surface has a first-order influence on the power output, while the temperature difference has a second-order influence. Therefore, the contribution of the additional contact surface does not outperform the loss from the temperature difference.

The internal structure also has a major impact on the heat transfer. The more solid the internal structure, the better heat transfer between the frame and the TEG, and the heavier the total weight would be.

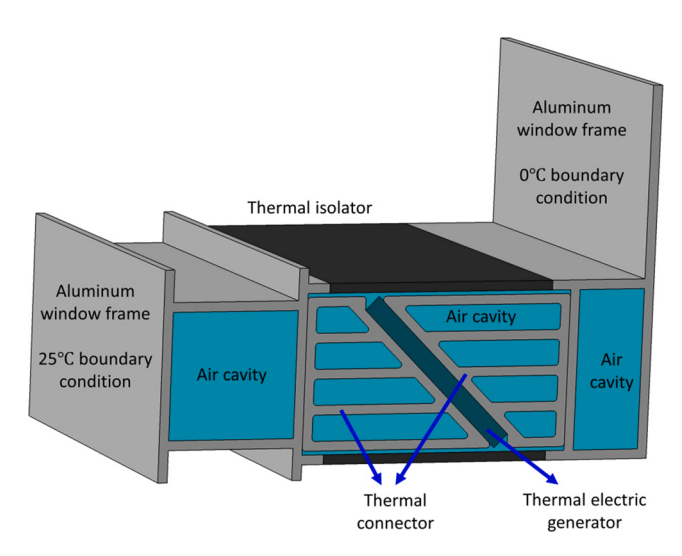


Fig. 6. Finite element model of the three-bridge 45 $^{\circ}\text{C}$ design.

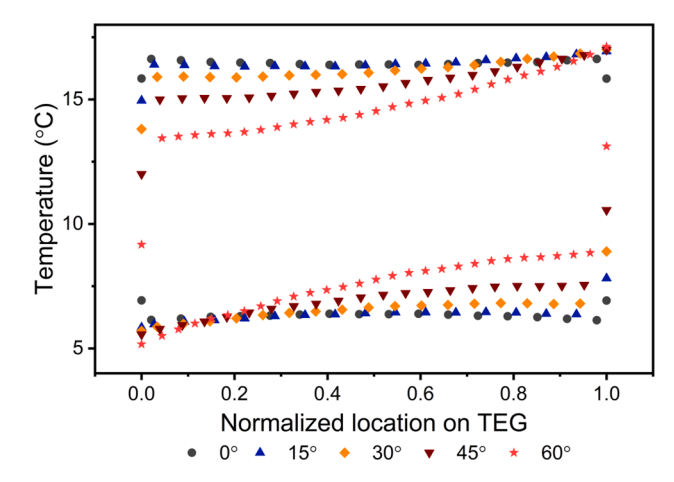


Fig. 7. Temperature profile on the two surfaces of TEG for the three-bridge design under different placement angles.

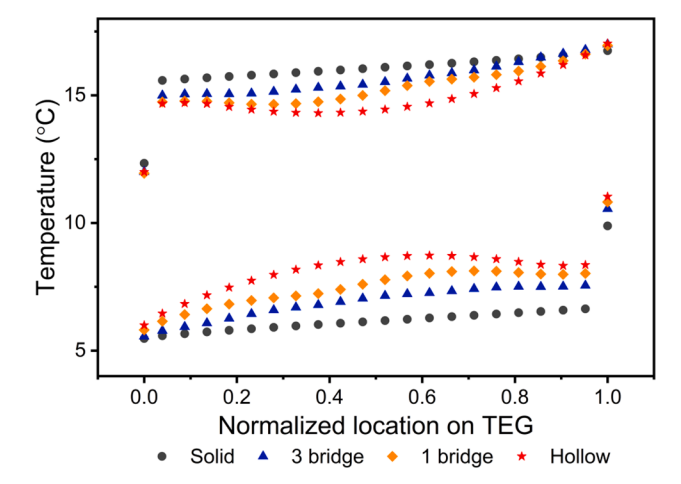


Fig. 8. Temperature profile on the two surfaces of TEG for the 45 $^{\circ}\text{C}$ angle design with different thermal connectors.

Therefore, it is coupled with how the weight is valued versus the power output. The scaling factor $\alpha=0$, 0.5, and 1 indicate that the additional weight has no influence, half as important, and equally important as the energy harvesting on the evaluation metric. Correspondingly, the best performing internal structure is the solid, the three-bridge, and the one-bridge structure. The hollow structure, although having the smallest weight, is outperformed by the one-bridge model when $\alpha=1$. When the scaling factor α is prescribed at 0.5, the three-bridge design is the optimal structure, which is selected for prototype fabrication.

The three-bridge structure with a 0-degree design generates the best performance when the scaling factor $\alpha=0.5$. Unfortunately, none of the commercial TEGs fit this dimension in the window frame. Therefore, the $30\text{mm}\times30\text{mm}\times3.7\text{mm}$ TEG is chosen for the prototype, which corresponds to the 45 °C placement angle. Four thermal connectors with a three-bridge internal structure and 45 °C TEG angle are manufactured by "i.materialise" using 3D printed aluminum. Fig. 10(A) shows the final energy harvester unit that contains two soldered TEGs and two 3D printed thermal connectors, with a depth of 60 mm. It replaces the original thermal resistive foam and is implemented inside the window frame, as illustrated in Fig. 10(B). The two sides of the energy harvester unit are attached to the two aluminum window frames to direct the temperature gradient from the window frame to the TEGs. In the prototype, two identical energy harvester units are implemented into the window frame, as is shown in Fig. 11, for thermal energy harvesting.

It is worth mentioning that the temperature variation along the

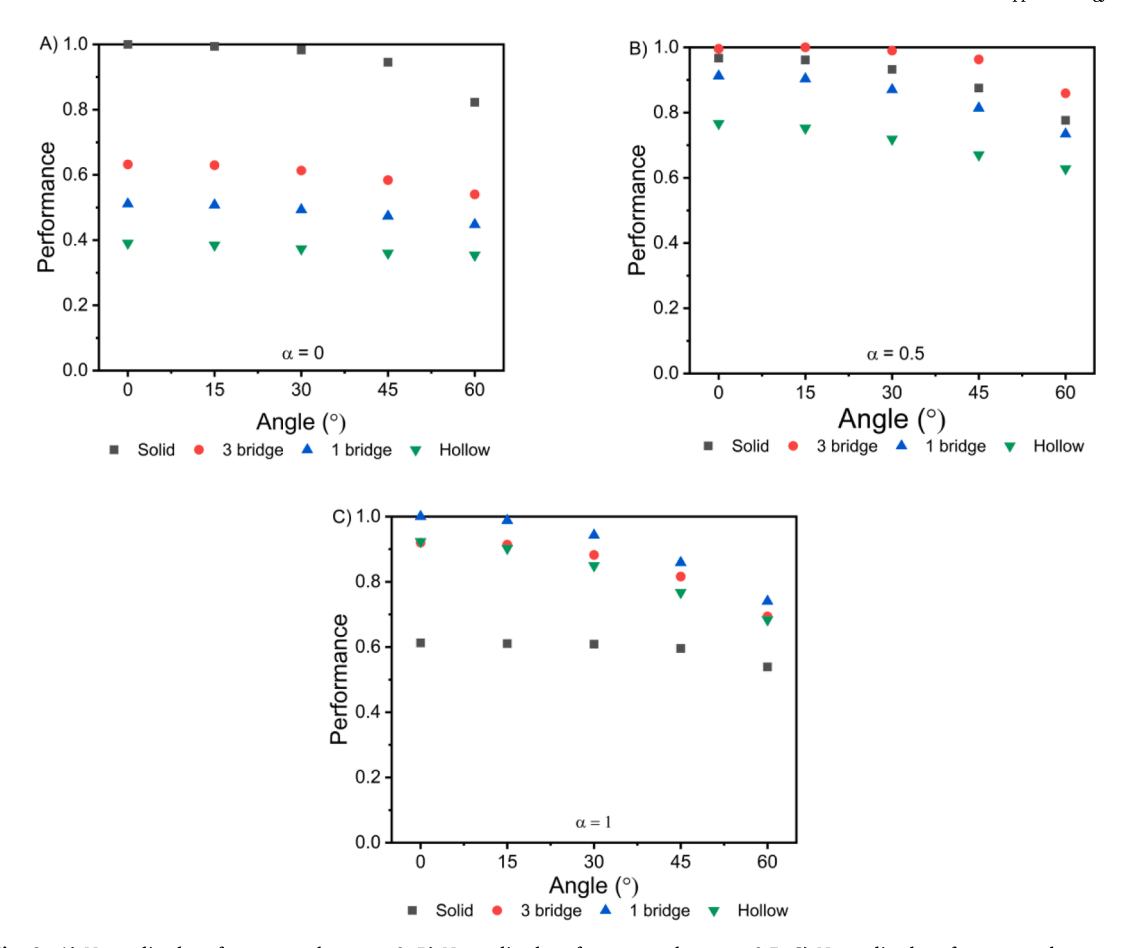
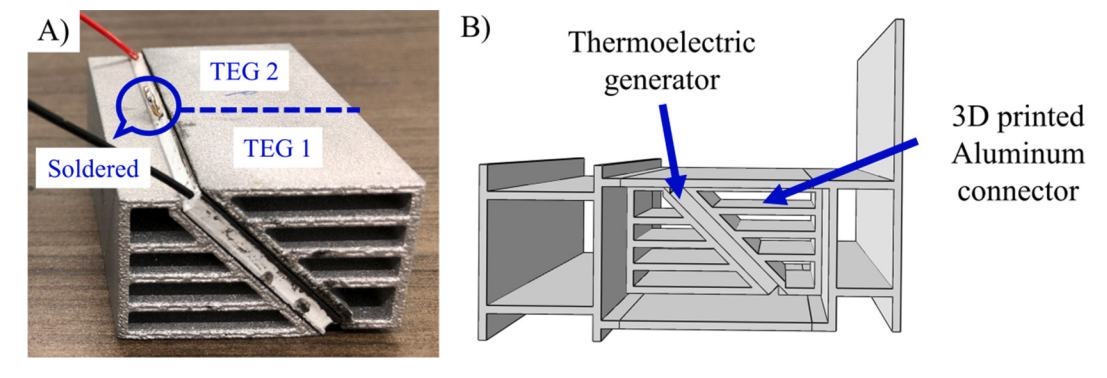


Fig. 9. A) Normalized performance when $\alpha=0$; B) Normalized performance when $\alpha=0.5$; C) Normalized performance when $\alpha=1.$



 $\textbf{Fig. 10.} \ \ A) \ \ \text{Energy harvester with two TEGs; B)} \ \ Position \ of \ the \ energy \ harvester \ unit \ inside \ the \ window \ frame.$

extrusion is not considered in the analysis. In a real application, the temperature varies bi-directionally both across the window profile and along the extrusion. The implemented TEG units will not only influence the window temperature profile but also interact with neighboring units. In 3D ABAQUS simulation, a single unit will influence the neighboring temperature profile up to the distance of a single unit's width, in both directions. Therefore, the TEG units could either be placed intermittently with the interval of twice the width to maximize its energy harvesting, or placed continuously to save the retrofitting cost, which requires further studies and trade-off analysis.

2.1.2. Battery and management circuits

The TEGs depend on the temperature difference for energy harvesting. However, the temperature difference is usually dynamic over time, which makes the power source unstable. Moreover, the voltage

output from TEGs is very small (usually tens of mV for the close circuit voltage) for building envelope applications, making it impossible to charge the battery alone. Therefore, a voltage regulator is needed to boost and stabilize the ultra-low input voltage to a battery charging voltage.

The LTC 3108 from Linear Technology is selected as the DC/DC converter to boost up the voltage from 20 mV to 5 V. The energy efficiency of the LTC 3108 is tested with the input voltage ranging from 50 mV to 1 V and plotted in Fig. 12, where a maximum efficiency at 70% is reached when the input is around 70 mV. The efficiency drops to 40% when the input voltage is 100 mV, and reduces with the increase of the input voltage. The LTC3108 is used for voltage boosting and regulation. A battery management circuit is also needed for permanent energy storage and battery protection.

The LTC4071 from Linear Technology is used as the battery man-

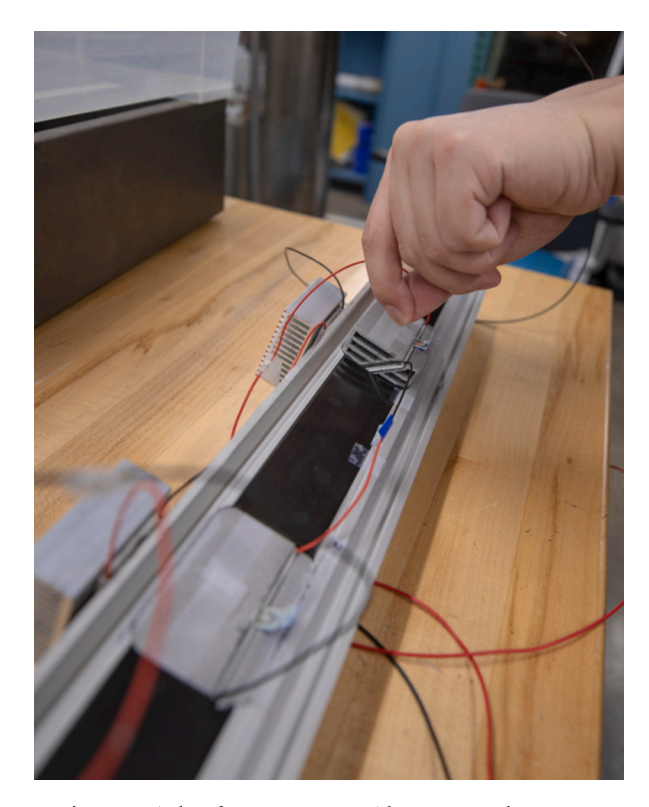


Fig. 11. Window frame prototype with two energy harvesters.

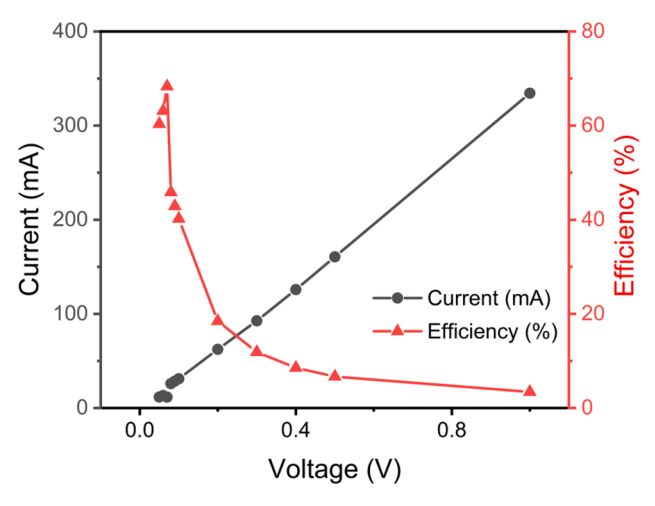


Fig. 12. LTC 3108 energy conversion efficiency.

agement circuit, which operates from 550nA to 50 mA. It allows the battery to charge from very low current under continuous and intermittent sources and provides overcharging and over-discharging protection. The circuit consumes 550 nA of operating current, and the averaged conversion efficiency is above 95%. Therefore, it is well suited to charge low-capacity Li-Ion or thin-film batteries in energy harvesting applications. The LTC4071 is used together with the LTC3108 to boost, regulate, and manage the voltage from TEGs to the battery. A diode is applied between LTC3108 and LTC4071 to control the current direction and avoid energy leaking. It is worth to mention that the LTC4071 controls the voltage of the whole circuit and that the LTC3108 output usually does not reach 5 V but depends on the need of the battery charging process.

The energy supply from TEG depends on the indoor and outdoor temperature and is dynamic across the year. Therefore, an energy storage unit is needed to store energy during peak season for consumption in the off-season. The Li-Po battery is used in this paper thanks to its high energy capacity, density, and efficiency. The 100 mAh battery is used during the lab test in Section 3.1 to capture and magnify the slow charging process. It is also concluded in Section 3.2 that a 500 mAh battery is large enough for New York to achieve the energy equilibrium stage. Since the unit is designed to stay inside the window frame for decades, the battery cycle life and the replacement cost shall be discussed before the real application but is currently not considered in this research.

2.2. Wireless sensor network subsystem

The energy harvesting unit extracts the energy from the ambient environment and feeds the wireless sensor network unit, which consists of the sensors, microprocessors, and wireless communication devices. A low-cost and low-energy-consumption sensor, DHT11, is selected for the temperature and moisture measurement. Various kinds of sensors can be applied if needed. The microcontroller ESP 32 FireBeetle is selected as the system-on-chip (SOC) for the data collection, preprocessing, and wireless communication. It is a model optimized in the deep sleep mode for the minimum energy consumption with the advertised current consumption as low as 10 μ A.The lowest measured consumption is approximately 50 μ A, but still outperforms the majority of the SOC in the market. The Wi-Fi is used to transport data to the clouds wirelessly.

As the brain of the system, the ESP 32 is responsible for the data reading, preliminary calculation, and wireless communication to external servers. The routines in ESP 32 are schematically shown in Fig. 13, which work in an infinite loop. After waking up from N mins deep sleep, the ESP 32 connects to the local Wi-Fi network and reads the signal from the connected sensors, after which it preprocesses the signal to a particular format and send it to an online proxy named IFTTT to log the data to Google Sheets. The IFTTT stands for 'If This Than That'. It is a web-based service provider which creates chains of conditional statements to help logging data to Google cloud services. The whole system goes to sleep again after confirming the receipt from IFTTT. The loop continues until the system is out of power.

A current shunt circuit is designed to monitor the current consumption with the data acquisition (DAQ) system. A 3.1 O resistor with a maximum power limit of five watts is used for voltage measurement. The ESP 32 is programmed to cycle at five minutes, and seven cycles are recorded with DAQ, with a sampling frequency of 10 Hz and the

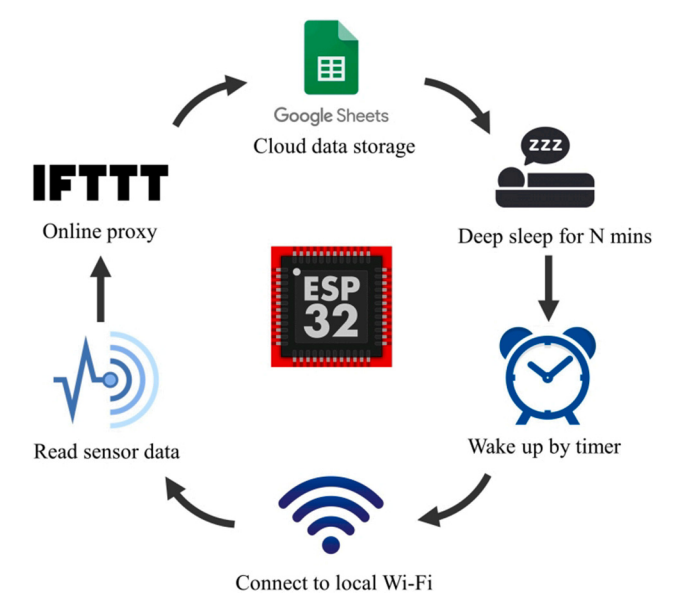


Fig. 13. Routines of the ESP 32.

measurement precision at 1×10^{-5} mA. Fig. 14 shows the current consumption in all seven cycles, while Fig. 15 shows a magnified consumption during the awake mode in the first cycle. It is clearly seen that the regular awake mode consumes approximately 40 mA, and the Wi-Fi mode consumes 115 mA. The average energy consumption is presented in Table 2, where the awake mode consumes approximately 70 mA while the deep sleep mode consumes 45 μ A. The average time needed for the awake mode is 7 s, which majorly depends on the connection speed to the local Wi-Fi network. Therefore, the total power consumed is calculated as:

$$P_{cycle} = \frac{V_{awake} \cdot I_{awake} \cdot t_{awake} + V_{sleep} \cdot I_{sleep} \cdot t_{sleep}}{t_{awake} + t_{sleep}}$$
(3)

The total power consumption can be tailored with the energy availability and the energy harvesting speed by controlling t_{sleep} .

A parametric study is conducted based on a 500 mAh battery and is shown in Table 3. It is seen that the power consumption reaches 0.42 mW when the deep sleep time is two hours, and the corresponding battery life is slightly more than half a year. Despite the low sampling frequency, battery life is still relatively short comparing to civil structures' service life. Therefore, energy harvesting is needed to achieve the energy equilibrium state.

Although ESP 32 is very energy efficient, its start-up current consumption reaches 450 mA, which could be a challenge for the system design. If the start-up current requirement were not met, the system could not start properly and will continuously leak energy until a manual reset or the battery depletion.

2.3. Energy equilibrium analysis

For traditional WSN systems, the system lifetime depends on how long the battery could last, after which the battery needs to be manually replaced to resume the service. In order to elongate the system lifetime, a naive design philosophy is to treat the harvested energy as a supplement to the batteries, while a more advanced philosophy is to use the harvested energy at an appropriate rate such that the system continues to operate perennially, which is so-called the energy-neutral operation [31]. A node is said to achieve the energy-neutral operation if the desired performance can be supported forever purely by the harvested energy. In order to achieve the energy-neutral state, many predictive models were proposed to forecast energy availability based on historical records [32]. Among them, the exponentially weighted moving-average (EMMA) method is one of the most straightforward models to predict future energy supply, such as the future solar power with local weather

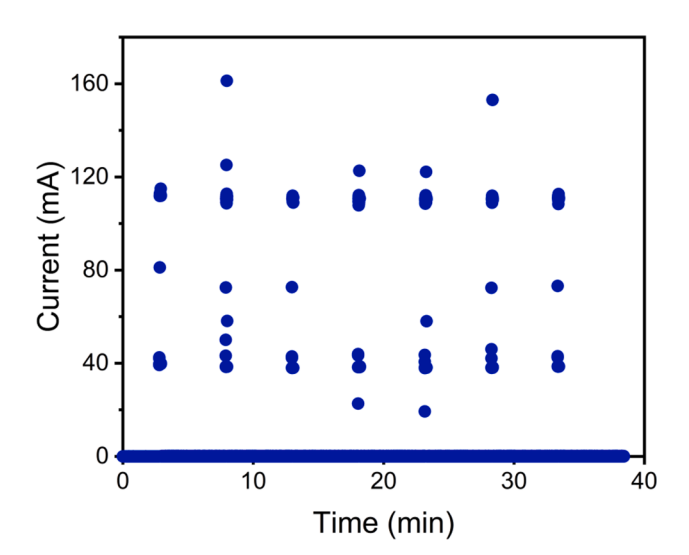


Fig. 14. ESP 32's awake and deep sleep current consumption.

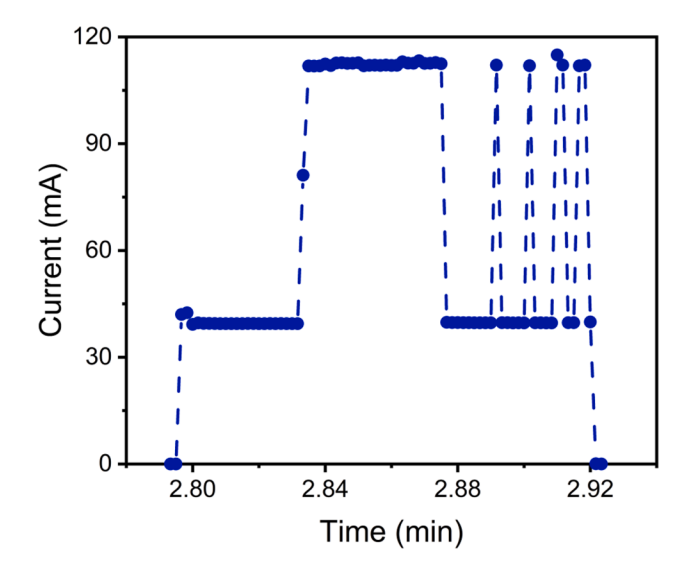


Fig. 15. ESP 32's awake current consumption in the first cycle.

conditions [33]. Apart from traditional methods, modern artificial intelligence methods such as the neural network [34], support vector [35], and tree-based models [36] were also used for future energy predictions. An accurate predictive model is useful for cases when the short-term parameter governs. For the TPWSN application, however, the governing parameter is the temperature difference between internal and external, which cycles over the period of a year. The complicated predictive models are no longer feasible considering the SOC's limited computational power. A practical and efficient approach is to engineer the historical temperature data, and apply a statistic safety factor. As long as the battery can survive the yearly cycling, the energy-neutral condition is satisfied, and the lifetime of a node will be extended without limits. In this section, an energy equilibrium algorithm is proposed based on the test measurements to predict the battery energy level, assuming that the historical temperature data is available and long enough to draw a statistical conclusion. A case study based on New York City's weather condition is conducted in Section 3.2 to guide the energy equilibrium design and engineering.

Two constraints for the battery level must be satisfied in order to achieve the energy equilibrium condition: a) the battery energy level cannot be below zero; b) the energy level of the battery is better to stay below the maximum capacity to avoid wasting of the harvested energy. The two constraints are written as:

$$\begin{cases} B(t) = B(0) + \int_{0}^{t} P_{H}(\xi) d\xi - \int_{0}^{t} P_{C}(\xi) d\xi - \int_{0}^{t} P_{leak} d\xi > 0, \exists t \in (0, T) \\ B(t) = B(0) + \int_{0}^{t} P_{H}(\xi) d\xi - \int_{0}^{t} P_{C}(\xi) d\xi - \int_{0}^{t} P_{leak} d\xi \leq \widehat{B}, \exists t \in (0, T) \end{cases}$$

$$(4)$$

where B(t) is the battery energy level at any time t and \widehat{B} is the maximum energy the battery can sustain; P_H, P_C and P_{leak} stand for the power of harvesting, consumption, and leakage of battery correspondingly; T is the time scale of the analysis.

The analysis based on continuous-time steps is necessary when the energy harvesting and consumption have close periods. For the case where the energy harvesting period (one year) is much longer than the prescribed energy consumption period (hours or minutes), the analysis in continuous time steps brings too much detail into the calculation. Such a problem can be avoided by analyzing discrete time steps. The constraints in Eq. (4) are converted to the corresponding discrete form as addressed below:

Table 2ESP 32's current consumption and awake time measurements.

Cycle	1	2	3	4	5	6	7	Average
Awake time (s)	7.5	6.1	6.1	8.4	8.3	6.2	6.2	7.0
Awake current (mA)	70.30	75.16	71.57	63.12	66.34	72.35	70.89	69.96
Deep sleep current (uA)	42.69	46.21	44.34	46.13	43.82	45.10	44.80	44.73

(5)

Table 3 Parametric study of battery life.

Deep sleep time	5 min	30 min	1 h	2 h	4 h
Averaged power consumption (mW)	6.07	1.17	0.67	0.42	0.29
500 mAh battery lifetime (day)	12.70	65.93	115.25	184.45	263.75

$$\begin{cases} B(t) = B(0) + \sum_{i=0}^{t/\Delta t} P_H(i) \Delta t - \sum_{i=0}^{t/\Delta t} P_C(i) \Delta t - \sum_{i=0}^{t/\Delta t} P_{leak} \Delta t > 0, \exists t \in (0, T) \\ B(t) = B(0) + \sum_{i=0}^{t/\Delta t} P_H(i) \Delta t - \sum_{i=0}^{t/\Delta t} P_C(i) \Delta t - \sum_{i=0}^{t/\Delta t} P_{leak} \Delta t \le \widehat{B}, \exists t \in (0, T) \end{cases}$$

where Δt is the prescribed time step for the analysis, e.g., $\Delta t = 1$ hour for the analysis based on the temperature measurement data with precision to 1 h. It is worth pointing out that Δt may not be the same with the period of energy consumption (e.g., the energy consumption loops every two hours, but the Δt can be one hour). The total time t may not be divisible by the step Δt , but since t is usually much larger than Δt , the remaining of the division has limited influence on the overall performance and is thus neglected in the equation.

For the energy harvesting based on the thermoelectric generator, the harvested power is linearly proportional to the area of the TEG surface A_{TEG} and the number of TEGs n_{TEG} . It is also quadratically proportional to the temperature difference ΔT_{TEG} , since both voltage and current are linearly dependent on the ΔT_{TEG} . Therefore, the power of energy harvesting is addressed as:

$$P_{H} = \frac{n_{TEG}}{n} \frac{A_{TEG}}{A_{TEG}} P_{H} \left(\frac{\Delta T_{TEG}}{\Delta T_{TEG}} \right)^{2} \eta \tag{6}$$

where η stands for the energy conversion efficiency in the voltage boosting, regulating and battery charging process, and • indicates the results and parameters measured in the test. For the TEGs integrated into the window frame, the temperature difference of TEG is directly related to the temperature difference of the window frame by the reduction factor λ :

$$\Delta T_{TEG} = \frac{\Delta T_{win}}{\lambda} \tag{7}$$

Therefore, the total energy harvested is addressed in the discrete form as:

$$\sum_{i=0}^{t/\Delta t} P_H(i) \Delta t = \sum_{i=0}^{t/\Delta t} \frac{n_{TEG}}{n} \frac{A_{TEG}}{A_{TEG}} P_H \left[\frac{\Delta T_{win}(i)}{\lambda \cdot \Delta T_{TEG}} \right]^2 \eta \Delta t \tag{8}$$

It is seen that only the window temperature difference ΔT_{win} is a function of time step i. All the other parameters are constant once the product configuration has been determined. The total energy harvested is therefore simplified into:

$$\sum_{i=0}^{t/\Delta t} P_H(i) \Delta t = \frac{n_{TEG}}{n} \frac{A_{TEG}}{A_{TEG}} P_H \frac{\eta \Delta t}{\lambda^2 \cdot \Delta T_{TEG}^2} \sum_{i=0}^{t/\Delta t} \Delta T_{win}^2(i)$$
(9)

The harvested energy is consumed by the wireless sensor network unit at the rate of P_C , which is an averaged value depending on the

awake mode P_a and the deep sleep mode P_s

$$P_C = \frac{P_a \cdot t_a + P_s \cdot t_s}{t_a + t_s} = P_s + (P_a - P_s) \frac{t_a}{t_a + t_s}$$
(10)

where t_a and t_s stand for the time spent during the awake mode and deep sleep mode, respectively. The awake mode is like the fixed cost of power, while the sleep mode is like the variable cost of power, which can be controlled to tailor the overall power consumption level. Since the P_a , P_s , and t_a cannot be manipulated, the only adjustable variable for power consumption is the deep sleep time t_s . The overall power consumption is inversely proportional to the deep sleep time and will gradually converges to the P_s with the increase of t_s . The total energy consumption is written as:

$$\sum_{i=0}^{t/\Delta t} P_C(i)\Delta t = \sum_{i=0}^{t/\Delta t} \left[P_s + (P_a - P_s) \frac{t_a}{t_a + t_s} \right] \cdot \Delta t \tag{11}$$

It is worth pointing out that the increase of the sleep time will compromise the data acquisition frequency and thus jeopardize the overall performance. Therefore, although the sleep time is adjustable, it could not exceed a certain design limit.

The power consumption is averaged over the cycle and that the consumption cycle may not coincide with the prescribed time step for the analysis. Therefore, the discrete form of the battery energy level is thus written as:

$$B(t) = B(0) + \frac{n_{TEG}}{n} \frac{A_{TEG}}{A_{TEG}} P_H \frac{\eta \Delta t}{\lambda^2 \cdot \Delta T_{TEG}^2} \sum_{i=0}^{t/\Delta t} \Delta T_{win}^2(i)$$

$$- \sum_{i=0}^{\frac{t}{\Delta t}} \left[P_s + (P_a - P_s) \frac{t_a}{t_a + t_s} \right] \cdot \Delta t - \sum_{i=0}^{t/\Delta t} P_{\text{leak}} \Delta t$$
(12)

The corresponding iterative form is written as:

$$B(m) = B(m-1) + \frac{n_{TEG}A_{TEG}}{n} P_H \frac{\eta \Delta t}{\lambda^2 \cdot \Delta T_{TEG}^2} \Delta T_{win}^2(m\Delta t)$$
$$- \left[P_s + (P_a - P_s) \frac{t_a}{t_a + t_s} \right] \cdot \Delta t - P_{leak} \Delta t$$
(13)

Once the initial condition B(0) is given, the battery energy level B(t) can be projected based on the temperature measurement data. The battery constraints in Eq. (5) shall be checked and followed during the analysis.

Since the temperature difference ΔT_{win} cycles at the period of a year, the projected battery energy B(t) fluctuates with the period of one year. The difference of the neighboring maximum and minimum ΔB_n gives the energy capacity needed for the year n and can be used to determine the battery's capacity. A straightforward way is to multiply the maximum difference by a safety factor as $\xi \cdot \max \Delta B_n$, which gives a good estimation when the historical data is limited. Another approach is to fit the historical difference $\Delta B_n (n=1,2,..N)$ into the Gaussian distribution so that the battery capacity can be determined with a prescribed confidence level.

3. Experiments and predictions

3.1. Experiments of TPWSN

Considering the milli-watt power from the thermal energy harvesting and the extremely small current after the voltage boosting, it is critical to

ensure that the tiny current is not wasted and can be accepted by the battery. Moreover, the harvested thermal energy must be larger than the consumed energy by the WSN node to fulfill the self-powered design objective. Therefore, the energy harvesting unit and the wireless sensor network unit are integrated in this subsection to formulate a complete TPWSN system for lab tests. The flow chart of the system is shown in Fig. 16. The harvested energy is first voltage-boosted by LTC3108 and then regulated by LTC4071 to charge the battery. A diode is applied to control the current direction so that it would not leak back to LTC3108. One 3.7 V 100 mAh Adafruit Lithium-Ion Polymer (Li-Po) battery is used for energy storage and supply to the wireless sensor network unit. In order to generate a stable temperature gradient across the window frame, the bottom surface of the window frame is immersed into the ice water for cooling, and the top surface is attached with controlled water flow for heating. The system is connected to a data acquisition system for continuous monitoring of the temperature profile and the battery energy, as is shown in Fig. 17.

The temperature of the water bath is controlled at 40 $^{\circ}$ C for a stable temperature profile across the window frame. Any other temperature will result in a monotonic increase or decrease over time. The charging of the battery is quantified by the increase of the battery's voltage. Since the amount of harvested energy is small, a small capacity battery is used to magnify the charging process so that the charging can be observed during the test.

Four thermocouples are implemented across the window profile, as indicated in Fig. 18. The temperature distributions over time are continuously monitored by the DAQ, with the sampling frequency of 2 Hz, which are plotted in Fig. 19. It is seen that under the warm water supply, the heat transfer across the window frame reaches a stable balance. The temperature measurements of four thermocouples are 24 °C, 11 °C, 5 °C, and 2.5 °C, corresponding to the top side of the window, the top side of the TEG, the bottom side of the TEG, and the bottom side of the window. The temperature difference ratio λ is defined

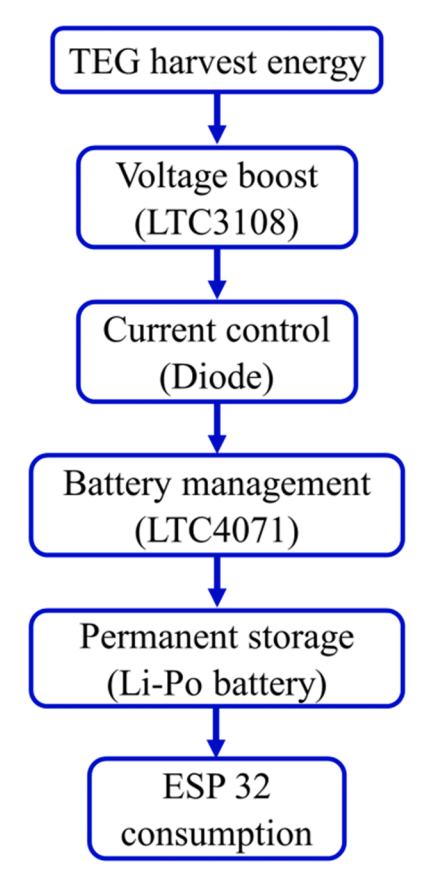


Fig. 16. Energy flow chart.

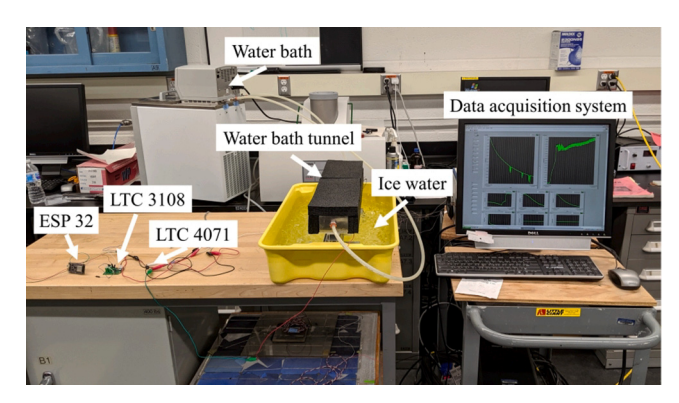


Fig. 17. Prototype test configuration.

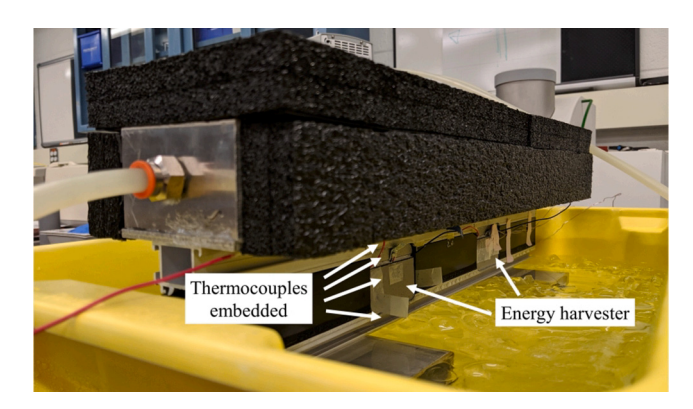


Fig. 18. Prototype with embedded thermocouples and controlled temperature gradations.

as the temperature difference of the window divided by the temperature difference of TEGs, $\lambda = \Delta T_{win}/\Delta T_{TEG}$. It is a function of the window's internal profile and independent of the external weather conditions. Therefore, $\lambda \cong 3.5$ as measured in the experiment is expected to remain stable in different weather configurations and can aid the energy equilibrium analysis.

The voltage output from four TEGs is measured and plotted against the temperature difference in Fig. 20, where a linear trend line of the measurement is observed. The voltage output stabilizes to 0.1 V given

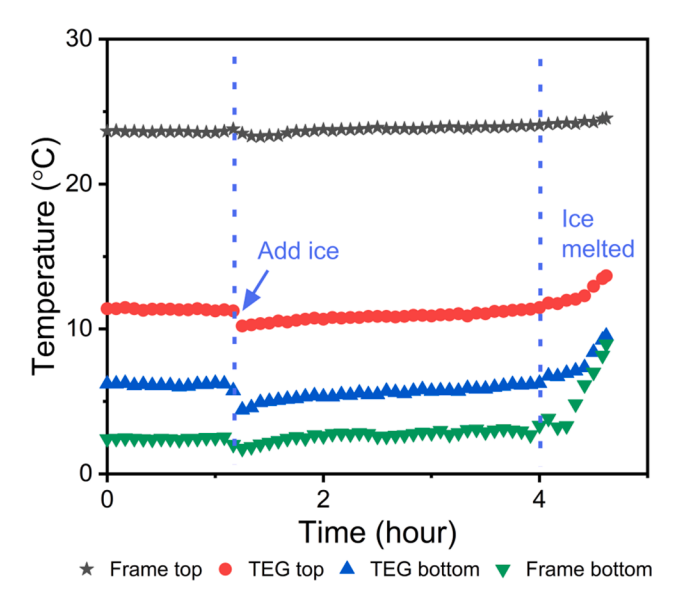


Fig. 19. Temperature distribution over time.

the 5 °C temperature difference across TEG surfaces. In order to obtain the current output from the TEGs, a separate test is conducted with a similar test configuration, except that the battery is changed to supercapacitors. The supercapacitor has a much lower energy density than the battery and can be fully charged by the TEGs in a few hours, so that the current can be calculated based on energy equilibrium. It is measured that 3 h are needed to fully charge two identical 2.7 V 1F supercapacitors. Considering the 40% conversion efficiency of the LTC3108 and the 100 mV voltage output from TEGs, the current output from the four TEGs is determined as 15 mA. Therefore, the total power output from four TEGs is calculated as $P = V \times I = 1.5$ mW.

The voltage and current measurements for every component are listed in Table 4, with the calculated power and the conversion efficiency. Since the battery has the highest energy density, it controls the circuit's voltage so that the LTC4071 will always have a voltage slightly over the battery's voltage. The diode takes 0.5 V of voltage with an efficiency of 88%. The 100 mV voltage output from TEGs is boosted by LTC3108 to 4.3 V with a 40% conversion efficiency, such that the battery can be charged. The total power into the battery is calculated at 0.51 mW, and the overall conversion efficiency is calculated as:

$$\eta = \eta_{3108} \times \eta_{diode} \times \eta_{4071} = 33.4\% \tag{14}$$

Therefore, the total energy that can be stored into the battery in an ESP 32's 2-hour cycle is 0.27 mAh.

The battery's voltage is continuously monitored by the DAQ and plotted in Fig. 21, with the measurement precision of $1\times 10^{-5} \rm V$. It is seen that the start-up of ESP 32 will quickly drain power from the battery, causing a significant drop in the measurement. After the ESP 32 enters the deep sleep mode, the battery's voltage gradually stabilizes and increases over time, which is plotted separately in Fig. 22. Approximately 0.001 V of battery voltage is raised in the 2 h charging cycle, indicating that the harvested energy outperforms the consumed energy in this specific testing configuration. It serves as a reference in the energy equilibrium modeling in the next subsection, where the engineering philosophy is discussed.

3.2. Energy equilibrium case study

Following the experiments discussed in the previous subsection, the parameters for energy harvesting are recorded as n=4, $A_{TEG}=A_{TEG}=9$ cm², $P_H=1.5$ mW, $\Delta \widetilde{T}_{TEG}=5$ °C, $\lambda\cong3.5$, and $\eta=\eta_{3108} \bullet \eta_{4071} \bullet \eta_{diode}=0.334$. The power consumption of the ESP 32 system is measured in section 2.2 with the voltage $V_{ESP32}=3.7$ V, awake current $I_a=70$ mA, and deep sleep current $I_s=45$ uA. The ESP 32 awake time is 7 s.

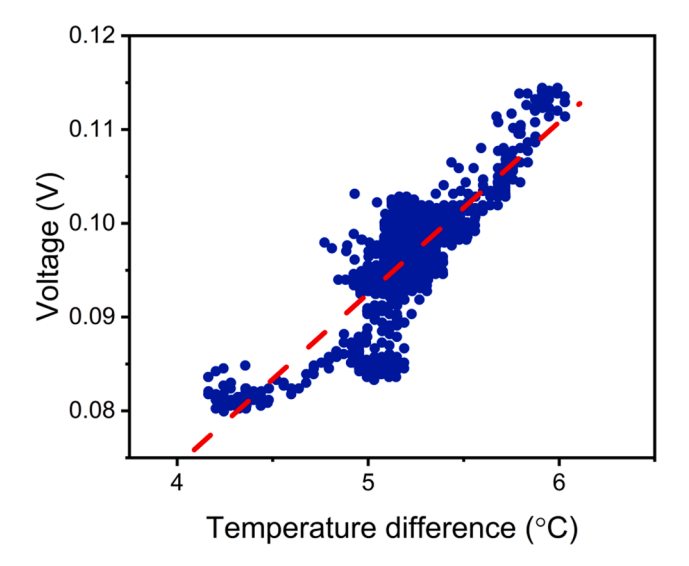


Fig. 20. The voltage output versus the temperature difference on TEG.

Table 4Voltage, current, and energy efficiency of the energy harvester.

	Voltage/mV	Current/mA	Power/mW	Efficiency
TEG	100	15	1.5	
LTC3108	4300	0.140	0.6	40%
Diode	3800	0.140	0.54	88%
LTC4071	3800	0.135	0.51	95%

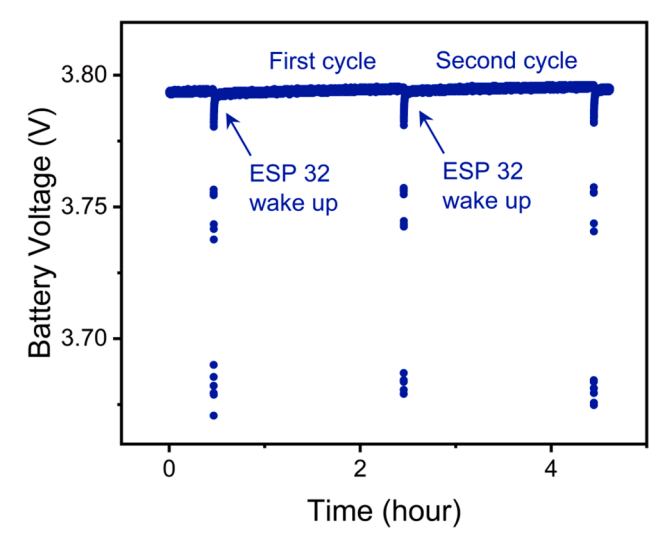


Fig. 21. Li-Po battery's voltage measurement over two cycles.

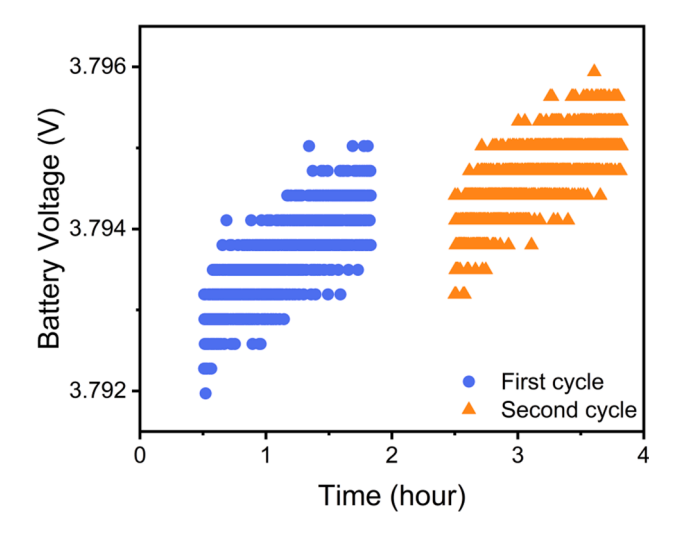


Fig. 22. Li-Po battery's charging process over two cycles.

It is seen from the energy equilibrium analysis that two variables, the number of TEGs n_{TEG} and the deep sleep time t_s , can be used to achieve the balance between harvesting and consumption.

The historical temperature data of New York City, as plotted in Fig. 23, is used for the energy equilibrium analysis. The per-hour temperature data is measured 2 m above ground in Central Park and lasts for 3.5 years from 2016 to 2019. The external window frame is assumed to have the same temperature as the environment, while the internal window frame has a temperature the same with the room temperature of 21 $^{\circ}$ C. Since the LTC3108 cannot take alternating current, the energy can only be harvested when the external temperature is lower than the internal temperature.

The energy equilibrium analysis is applied to predict the battery energy level based on the historical temperature data. In the case study,

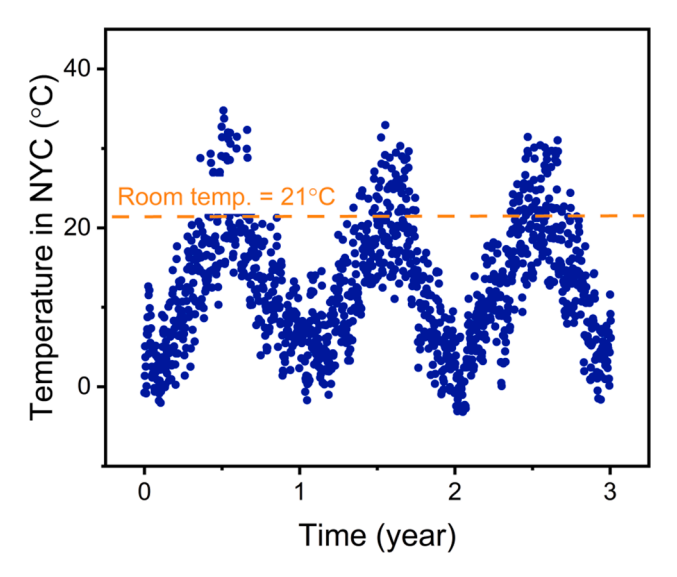


Fig. 23. New York City historical temperature profile.

the initial battery level is prescribed at 100 mAh. The system is assumed to deploy on the first day of a year, when the ambient temperature is low. The battery energy predictions based on different t_s and n_{TEG} are determined and plotted in Fig. 24. It is seen that the energy equilibrium state can be achieved by parametric studies. The battery capacity can also be determined by looking at the local maximum and minimum in a single cycle. The rule of thumb for the energy equilibrium design is to choose a slightly upgrowing curve to avoid the battery depletion and minimize waste. Among the four scenarios, the case with $t_s = 2$ hrs and $n_{TEG} = 4$ can achieve the balance between energy harvesting and consumption without wasting too much energy. For building applications, the frequency requirement for data acquisition is relatively low. One measurement in one or two hours is already enough for many applications. The $n_{TEG} = 4$ takes 120 mm length of window profile and is equivalent to 3% the extrusion length of a typical 1 m²-sized window. For large-sized windows or modern facade structures, it is very easy to get an extrusion length of more than 8 m. Therefore, if a higher sampling frequency is needed, more energy harvesting units can be implemented to increase the harvested energy.

Given the local temperature data, the parameter t_s and n_{TEG} can be properly engineered to achieve the self-powered goal at any location. The difference between the maximum and the minimum battery energy ΔB_i can be determined easily from the prediction in Fig. 24, such that the

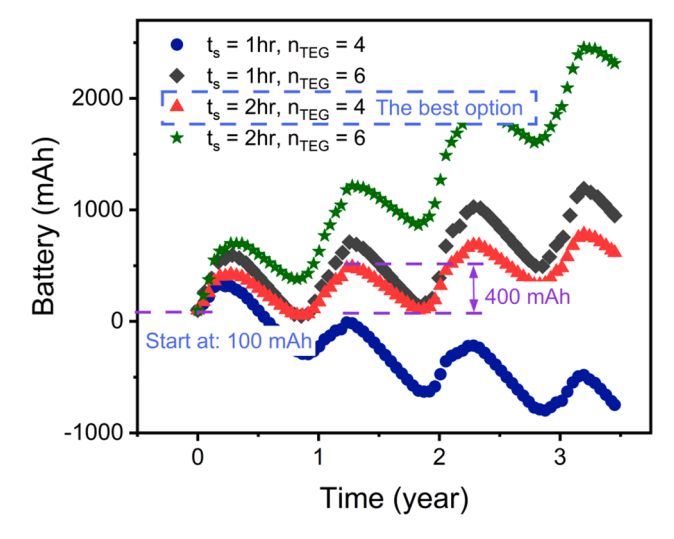


Fig. 24. Battery energy predictions for TPWSN system in New York City.

battery capacity can be calculated by multiplying the maximum difference $\max \Delta B_i = 400 \text{mAh}$ by a safety factor ξ . Therefore, a 500 mAh battery is selected, assuming a 125% safety factor. It is worth mentioning that the battery's initial energy level depends majorly on the deployment date. The 100 mAh initial energy is used in this case study as an example, which works well since the deployment data is in winter and the harvesting is stronger than the consumption. If the system is installed in summer, more initial energy is needed to cover the consumption till the harvesting seasons, so that the battery will not deplete. A more conservative approach is to fully charge the battery before deployment.

4. Discussion

4.1. Cost analysis

The proposed TPWSN system's material costs are listed in Table 5, with corresponding part numbers and vendor information. The total costs add up to \$182.3 for a single TPWSN system with two energy harvesters and one wireless sensor network unit, which is very close to its battery-powered WSN competitors [37,38]. However, significant amounts of manpower and replacement cost during installation and maintenance could be saved thanks to the self-powered design, which contributes to the long-term return on investment. The thermoelectric generator has the maximum percentage cost. If only one energy harvester is used for a TPWSN system, the total cost is brought down to \$110, at the expense of a slightly smaller sampling frequency. It is also worth mentioning that the thermal connectors is manufactured with 3D printed aluminum, which costs more than \$250 for each piece. Such cost will be significantly reduced to a value close to the material cost with the metal extrusion during mass production. Therefore, it is estimated as the Aluminum material cost times a markup of 150% to cover then manufacturing and logistic.

4.2. Limitations and future work

The proposed TPWSN system harvests thermoelectric energy across the window frame for sensors and microcontrollers. It sits entirely inside the window frame and is independent of external weather conditions. However, some limitations are observed and deserve future improvements. First of all, the thermoelectric energy harvester is highly customized to the window frames, making it less robust to other building applications. In comparison, the power management and wireless sensor network subsystems are more robust to other SPWSNs applications. Another major challenge is the potential compromise of the window's original thermal and waterproof performance. The thermal compromise is less significant since only a small portion of the original thermal resistive foam is replaced by the TPWSN. However, the proposed TPWSN will change the window's internal temperature profile, which

Table 5Material cost breakdown of the TPWSN system.

Function	Parts	Vendor	#	Unit price (\$)	Total price (\$)
Sensor	DHT 11	Adafruit	1	5	182.30
Micro-controller	ESP 32 FIREBEETLE	DFRobot	1	18	
Voltage booster	LTC 3108	Linear Tech	1	8	
Battery management	LTC 4071	Linear Tech	1	6	
Battery	500 mAh battery	Adafruit	1	8	
Thermoelectric generator	1261G-7L31- 04CL	Custom Thermoelectric	4	34.2	
Thermo connector	-	-	4	0.12	

impacts the water condensation inside the window frame. Therefore, it might introduce potential water leakage and short current to the system. From a market perspective, the proposed system is designed for newly manufactured window frames and is not robust to retrofitting the existing windows. More investigations are needed to provide a solution for existing windows with different profiles.

5. Conclusions

This paper presents the design of a thermoelectric-powered wireless sensor network system inside a window frame and demonstrates its potentials for the next generation of smart building envelope systems. The self-powered design is achieved by balancing the harvested and consumed energy and is validated by the lab test. The corresponding energy equilibrium analysis is proposed to achieve the balance in any geographic location with appropriate engineering of variables. The case study based on New York City demonstrated that the self-powered design could be achieved with two energy harvesting units and one measurement every two hours. The low sampling frequency is usually enough for many building envelope applications but could be increased by adding more energy harvesting units. The key system performance and features are listed as follows:

- The optimized internal structure is proposed to maximize the temperature difference on thermoelectric generator's surfaces based on heat transfer analysis in Abaqus.
- 5.1 mW thermoelectric power could be harvested based on 6 °C of temperature difference on 9cm² of thermoelectric generator.
- A voltage boosting integrated circuit (LTC3108) and a battery management circuit (LTC4071) are required to boost up and regulate the ultra-small voltage for battery charging, which provides a 33.4% energy conversion rate from thermoelectric generators to the battery.
- The power consumption depends on the ratio of awake and deep sleep time and can be as low as 0.42 mW for one measurement every two hours.
- The sensor data is wirelessly transferred to Google Sheet through the local Wi-Fi network, which could be changed to Bluetooth Low Energy for lower energy consumption.
- Energy equilibrium algorithm is proposed based on the test data, based on which 9cm² of thermoelectric generators provides enough power for the proposed system to work in New York City's weather condition.
- The energy equilibrium design does not have a unique solution, and the variables can be modified to accommodate the design and engineering needs.
- The proposed system is robust to various sensors and informs the next generation of the smart building envelope systems.

Further studies are needed to quantify the impact of the proposed system on the internal temperature profile, so as to eliminate the potential water condensation inside the window frame. The retrofitting of the existing window systems also deserves further investigation, such that a much larger market could be available for future applications.

CRediT authorship contribution statement

Qiliang Lin: Methodology, Data curation. **Yi-Chung Chen:** Methodology, Supervision. **Fangliang Chen:** Conceptualization, Project administration. **Tejav DeGanyar:** Conceptualization, Project administration. **Huiming Yin:** Funding acquisition, Conceptualization, Project administration, Writing – review & editing.

Declaration of Competing Interest

The authors declare that they have no known competing financial

interests or personal relationships that could have appeared to influence the work reported in this paper.

Acknowledgement

This study has been sponsored by the NSF IIP 1941244 and 1738802 - IUCRC Center for Energy Harvesting Materials and Systems (CEHMS), for the industry-university cooperative project with Schüco USA, whose supports are gratefully acknowledged. The authors appreciate Dr. Liming Li on the experimental tests.

References

- [1] US Department of Energy. Quadrennial Technology Review 2015 An Assessment of Energy Technologies and Research Opportunities. US Dep Energy 2015.
- [2] Manic M, Wijayasekara D, Amarasinghe K, Rodriguez-Andina JJ. Building Energy Management Systems: The Age of Intelligent and Adaptive Buildings. IEEE Ind Electron Mag 2016;10(1):25–39. https://doi.org/10.1109/MIE.2015.2513749.
- [3] Energy Information Administration (EIA). Annual Energy Review 2014-With Projections to 2040. Washington, DC: U.S: Department of Energy; 2014.
- [4] Kroner WM. An intelligent and responsive architecture. Autom Constr 1997;6(5-6): 381–93. https://doi.org/10.1016/S0926-5805(97)00017-4.
- [5] Wigginton M, Harris J. Intelligent Skins. Routledge; 2013.
- [6] Yang J, Peng H. Decision support to the application of intelligent building technologies. Renew Energy 2001;22(1-3):67–77. https://doi.org/10.1016/S0960-1481(00)00085-9.
- Böke J, Knaack U, Hemmerling M. State-of-the-art of intelligent building envelopes in the context of intelligent technical systems. Intell Build Int 2019;11(1):27–45. https://doi.org/10.1080/17508975.2018.1447437.
- [8] Berawi MA, Miraj P, Sayuti MS, Berawi ARB. Improving building performance using smart building concept: Benefit cost ratio comparison. AIP Conf Proc 2017; 1903:030001. https://doi.org/10.1063/1.5011508.
- [9] Global Smart Home Market Size 2016: Industry Analysis & Trends Up to 2022 n.d. https://www.zionmarketresearch.com/report/smart-home-market?utm_source =joseph/FREE/SM/jump (accessed April 23, 2020).
- [10] Shaikh PH, Nor NBM, Nallagownden P, Elamvazuthi I, Ibrahim T. A review on optimized control systems for building energy and comfort management of smart sustainable buildings. Renew Sustain Energy Rev 2014;34:409–29. https://doi. org/10.1016/j.rser.2014.03.027.
- [11] Marino DL, Amarasinghe K, Manic M. Building energy load forecasting using Deep Neural Networks. IECON 2016–42nd Annu. Conf. IEEE Ind. Electron. Soc. 2016: 7046–51. https://doi.org/10.1109/IECON.2016.7793413.
- [12] Wang L, Lee EWM, Yuen RKK. Novel dynamic forecasting model for building cooling loads combining an artificial neural network and an ensemble approach. Appl Energy 2018;228:1740–53. https://doi.org/10.1016/j. apenergy.2018.07.085.
- [13] Raza MQ, Khosravi A. A review on artificial intelligence based load demand forecasting techniques for smart grid and buildings. Renew Sustain Energy Rev 2015;50:1352–72. https://doi.org/10.1016/j.rser.2015.04.065.
- [14] Chen Z, Jiang C, Xie L. Building occupancy estimation and detection: A review. Energy Build 2018;169:260–70. https://doi.org/10.1016/j.enbuild.2018.03.084.
- [15] Kazmi AH, O'grady MJ, Delaney DT, Ruzzelli AG, O'hare GMP. A Review of Wireless-Sensor-Network-Enabled Building Energy Management Systems. ACM Trans Sen Netw 2014;10(4):1–43. https://doi.org/10.1145/2532644.
- [16] Maharjan P, Salauddin M, Cho H, Park JY. An indoor power line based magnetic field energy harvester for self-powered wireless sensors in smart home applications. Appl Energy 2018;232:398–408. https://doi.org/10.1016/j. apenergy.2018.09.207.
- [17] Jelle BP. Building Integrated Photovoltaics: A Concise Description of the Current State of the Art and Possible Research Pathways. Energies 2016;9:21. https://doi. org/10.3390/en9010021.
- [18] Chen J, Qiu Q, Han Y, Lau D. Piezoelectric materials for sustainable building structures: Fundamentals and applications. Renew Sustain Energy Rev 2019;101: 14–25. https://doi.org/10.1016/j.rser.2018.09.038.
- [19] Pan Yu, Lin T, Qian F, Liu C, Yu J, Zuo J, et al. Modeling and field-test of a compact electromagnetic energy harvester for railroad transportation. Appl Energy 2019; 247:309–21. https://doi.org/10.1016/j.apenergy.2019.03.051.
- [20] Gao M, Wang Y, Wang Y, Wang P. Experimental investigation of non-linear multistable electromagnetic-induction energy harvesting mechanism by magnetic levitation oscillation. Appl Energy 2018;220:856–75. https://doi.org/10.1016/j. apenergy.2018.03.170.
- [21] Ando Junior OH, Maran ALO, Henao NC. A review of the development and applications of thermoelectric microgenerators for energy harvesting. Renew Sustain Energy Rev 2018;91:376–93. https://doi.org/10.1016/j.rser.2018.03.052.
- [22] Matiko JW, Grabham NJ, Beeby SP, Tudor MJ. Review of the application of energy harvesting in buildings. Meas Sci Technol 2014;25(1):012002. https://doi.org/ 10.1088/0957-0233/25/1/012002.
- [23] Tzortzakis K, Papafotis K, Sotiriadis PP. Wireless self powered environmental monitoring system for smart cities based on LoRa. 2017 Panhellenic Conf. Electron. Telecommun. PACET, 2017, p. 1–4. 10.1109/PACET.2017.8259970.
- [24] Wang Wensi, Cionca Victor, Wang Ningning, Hayes Mike, O'Flynn Brendan, O'Mathuna Cian. Thermoelectric Energy Harvesting for Building Energy

- Management Wireless Sensor Networks. Int J Distrib Sens Netw 2013;9(6):232438. https://doi.org/10.1155/2013/232438.
- [25] Guan M, Wang K, Xu D, Liao W-H. Design and experimental investigation of a low-voltage thermoelectric energy harvesting system for wireless sensor nodes. Energy Convers Manag 2017;138:30–7. https://doi.org/10.1016/j.enconman.2017.01.049.
- [26] Lin Y-H, Tsai K-T, Lin M-D, Yang M-D. Design optimization of office building envelope configurations for energy conservation. Appl Energy 2016;171:336–46. https://doi.org/10.1016/j.apenergy.2016.03.018.
- [27] Chen F, Yin H. Fabrication and laboratory-based performance testing of a building-integrated photovoltaic-thermal roofing panel. Appl Energy 2016;177:271–84. https://doi.org/10.1016/j.apenergy.2016.05.112.
- [28] Lin Qiliang, Zhang Yanchu, Mieghem Arnaud Van, Chen Yi-Chung, Yu Nanfang, Yang Yuan, et al. Design and experiment of a sun-powered smart building envelope with automatic control. Energy Build 2020;223:110173. https://doi.org/10.1016/ i.enbuild.2020.110173.
- [29] Hassanli S, Hu G, Kwok KCS, Fletcher DF. Utilizing cavity flow within double skin façade for wind energy harvesting in buildings. J Wind Eng Ind Aerodyn 2017;167: 114–27. https://doi.org/10.1016/j.jweia.2017.04.019.
- [30] Bekkouche SMA, Cherier MK, Hamdani M, Benamrane N, Benouaz T, Yaiche MR. Thermal resistances of air in cavity walls and their effect upon the thermal insulation performance. Int J Energy Environ Print 2013;4.
- [31] Kansal Aman, Hsu Jason, Zahedi Sadaf, Srivastava Mani B. Power management in energy harvesting sensor networks. ACM Trans Embed Comput Syst 2007;6(4):32. https://doi.org/10.1145/1274858.1274870.
- [32] Shaikh FK, Zeadally S. Energy harvesting in wireless sensor networks: A comprehensive review. Renew Sustain Energy Rev 2016;55:1041–54. https://doi. org/10.1016/j.rser.2015.11.010.

- [33] Recas Piorno J, Bergonzini C, Atienza D, Simunic Rosing T. Prediction and management in energy harvested wireless sensor nodes. 2009 1st Int. Conf. Wirel. Commun. Veh. Technol. Inf. Theory Aerosp. Electron. Syst. Technol., 2009, p. 6–10. 10.1109/WIRELESSVITAE.2009.5172412.
- [34] Rodríguez F, Fleetwood A, Galarza A, Fontán L. Predicting solar energy generation through artificial neural networks using weather forecasts for microgrid control. Renew Energy 2018;126:855–64. https://doi.org/10.1016/j.renene.2018.03.070.
- [35] Fazavi Mohammad, Hosseini Seyyed Mohsen, Arabloo Milad, Shokrollahi Amin, Nouri-Taleghani Morteza, Amani Mahmood. Applying a Smart Technique for Accurate Determination of Flowing Oil-Water Pressure Gradient in Horizontal Pipelines. J Dispers Sci Technol 2014;35(6):882–8. https://doi.org/10.1080/ 01932691.2013.805653.
- [36] Ahmad MW, Mourshed M, Rezgui Y. Tree-based ensemble methods for predicting PV power generation and their comparison with support vector regression. Energy 2018;164:465–74. https://doi.org/10.1016/j.energy.2018.08.207.
- [37] Vikram N, Harish KS, Nihaal MS, Umesh R, Kumar SAA. A Low Cost Home Automation System Using Wi-Fi Based Wireless Sensor Network Incorporating Internet of Things (IoT). 2017 IEEE 7th Int. Adv. Comput. Conf. IACC, 2017, p. 174–8. 10.1109/IACC.2017.0048.
- [38] Mondal A, Misra IS, Bose S. Building a low cost solution using wireless sensor network for agriculture application. 2017 Int. Conf. Innov. Electron. Signal Process. Commun. IESC, 2017, p. 61–5. 10.1109/IESPC.2017.8071865.
- [39] Berkovsky, B. M., and Polevikov, V. K., 1977, Numerical Study of Problems on High-Intensive Free Convection, Heat Transfer and Turbulent Buoyant Convection: Studies and Applications for Natural Environment, Buildings, Engineering Systems, Hemisphere Publishing, Washington, DC, pp. 443–455.